Supplementary Material:

1. Description of the new unified treatment of aerosol processing by convective clouds

We begin by briefly reviewing the existing CAM5 treatment. The treatments of deep and shallow convective clouds in CAM5 are described at length in Neale et al. (2010) and references therein. The deep convection parameterization is based on Zhang and McFarlane (1995), and considers an ensemble of updraft and downdraft plumes, although only the ensemble updraft and downdraft properties are used for aerosol processing. The shallow convective parameterization is based on Park and Bretherton (2009), represented by a single entraining-detraining updraft plume. From the standpoint of aerosol processing, the deep and shallow convection treatments are conceptually very similar. Also, both of the existing treatments of aerosol processing by convective clouds consider wet removal and vertical transport separately and sequentially.

The wet removal of aerosols in CAM5 distinguishes between "in-cloud wet removal" (activation of interstitial aerosol particles to become cloud-borne aerosol, following by conversion of cloud-condensate and cloud-borne aerosol to precipitation) and "below-cloud wet removal" (capture of interstitial aerosol particles by precipitation particles via impaction and Brownian diffusion). Below-cloud wet removal is identical in the existing and new unified treatments. Note that CAM5 treats cloud-borne aerosols within stratiform clouds explicitly in a prognostic manner, and they are assumed to not interact with convective clouds. The "interstitial" aerosol mixing ratios in the CAM5 code ($\overline{q}_{AI*}$) are defined to be the sum of interstitial plus convective-cloud-borne aerosols, expressed as grid-cell averaged quantities. The convective-cloud-borne aerosols are calculated in the wet removal routines in a diagnostic manner.

The in-cloud aerosol wet removal parameterizations for shallow and deep convection utilize profiles of cloud fractional area (f_{CLDC}), in-cloud cloud-condensate mixing ratio (*ICWMR*, in kg kg^{-1}), and grid-cell mean precipitation production (*RPROD*, in kg kg^{-1} s^{-1}), to calculate a first-order rate loss rate (the rate at which cloud-condensate is converted to precipitation within the cloud),

$$\lambda_{WETC} = RPROD \,/\, (f_{CLDC}\ ICWMR)\ . \qquad \text{(S1)}$$

In the CAM5 convective-cloud wet removal, the cloud-borne aerosol mixing ratio within the convective cloud is assumed equal to the grid-cell mean interstitial aerosol mixing ratio at that level multiplied by a prescribed convective-cloud activation fraction, f_{ACTC}, which varies with aerosol mode and species. Over a model time-step Δt, a fraction $f_{WETC} = \text{MIN}(\ \Delta t \cdot \lambda_{WETC},\ 1\ )$ of this cloud-borne aerosol is removed, and the change to the grid-cell mean interstitial aerosol is

$$\Delta \overline{q}_{AI*} = -0.4\, f_{CLDC}\, f_{WETC}\, f_{ACTC}\, \overline{q}_{AI*} \qquad \text{(S2)}$$

where the 0.4 is a wet removal adjustment factor, applied because f_{CLDC} and f_{WETC} from the convective parameterizations would otherwise produce too much wet removal.

The deep convective vertical transport of aerosols and other trace species follows the assumption in the original ZM parameterization that the updrafts and downdrafts are described by steady-state bulk plume models representing the ensemble of up- and downdrafts in the clouds. Aerosol mixing ratios in the updraft ($q_{A,U}$) and downdraft ($q_{A,D}$) ensembles are calculated by integrating steady-state mass continuity equations either upwards or downwards:

$$\frac{\partial\left(M_U\ q_{A,U}\right)}{\partial p} = E_U\left(1 - f_{WET}\right) q_{A,E} - D_U\, q_{A,U} \qquad \text{(S3a)}$$

$$\frac{\partial(M_D\, q_{A,D})}{\partial p} = E_D\,(1 - f_{WET})\, q_{A,E} - D_D\, q_{A,D} \qquad \text{(S3b)}$$

Here the *U*, *D*, and *E* subscripts denote updraft, downdraft, and environment, *M* is vertical mass flux of air (Pa s^{-1}), *E* is the positive portion of $\partial M/\partial p$ due to entrainment, $-D$ is the negative portion due to detrainment, *p* is pressure, and f_{WET} is the fractional wet removal of aerosols in the convective and stratiform clouds areas. The $(1-f_{WET})$ factor applied to entrainment accounts for wet removal of aerosols that is applied prior to the deep convective transport, providing some coupling of wet removal and vertical transport. Also, $q_{A,E}$ is assumed equal to $\overline{q}_{AI*}$. Equations S3a and S3b are solved to determine mixing ratios in the convective up- and downdrafts. The grid-cell mean interstitial plus convective-cloud-borne aerosol mixing ratios are then updated by solving

$$\frac{\partial \overline{q}_{AI*}}{\partial t} = -\frac{\partial}{\partial p}\left[M_U\, q_{A,U} + M_D\, q_{A,D} + M_E\, q_{A,E}\right] \qquad \text{(S4)}$$

where $M_E = -(M_U + M_D)$ is the compensating vertical mass flux in the environment. The shallow convective transport of aerosols is treated similarly, but the $(1-f_{WET})$ factor is not applied to entrainment, there is no downdraft, and the numerical discretization applied to the (S3-4) differs somewhat.

The main differences between the new unified treatment of aerosol processing by convective clouds and the previous CAM5 treatments are that (1) wet removal and vertical transport are treated simultaneously, (2) cloud-borne aerosols and aerosol activation are treated explicitly in the updraft, and (3) wet removal is applied to aerosols in the updraft. Similar to the previous

treatments, we assume that aerosol mixing-ratio profiles in the updraft and downdraft are steady-state. The mass-continuity equation for the updraft is:

$$\frac{\partial\left(M_U\, q_{AX,U}\right)}{\partial p} = E_U\, q_{AX,E} - D_U\, q_{AX,U} + A_U\,(\dot{q}_{AX,U})_{ACT} + A_U\,(\dot{q}_{AX,U})_{WET} \qquad \text{(S5)}$$

where the *AX* subscript is either *AI* for an interstitial aerosol species or *ACC* for a convective-cloud-borne (activated) aerosol species. (Note that q_{AI} is interstitial aerosol only, while $\overline{q}_{AI*}$ includes the convective-cloud-borne aerosol.) The $(\dot{q}_{AX,U})_{ACT}$ and $(\dot{q}_{AX,U})_{WET}$ terms are the rates of change due to activation and in-cloud wet removal in the updraft, respectively. For the downdraft, we assume that only interstitial aerosol is entrained from the environment and there is no aerosol activation as the downdraft is never super-saturated. As a result, the downdraft contains only interstitial aerosol, and there is no in-cloud wet removal. Thus the downdraft mass-continuity equation is unchanged from (S3b).

Aerosol activation in the updraft includes activation at cloud-base and above cloud-base. The cloud-base activation uses the Abdul-Razzak and Ghan (2000) parameterization to diagnose the maximum supersaturation in a rising air parcel and the activation fraction (f_{ACTC}) for interstitial aerosol mass and number of each aerosol mode. This requires an updraft vertical velocity, w_U, which can be diagnosed from $M_U = \rho\, A_U\, w_U\, g$, where ρ is air density, A_U is updraft fractional area, and g is the gravitational constant. The shallow convection parameterization assumes that $A_U = f_{CLDC}/2$, and this gives reasonable values for w_U. The deep convection parameterization provides no information on A_U, and using $A_U = f_{CLDC}/2$ gives unreasonably low values for w_U. Thus for deep convection we use empirical values for w_U based on measurements by Zipser and Lemone (1980) during GATE. The activation tendency needed in (S5) is then

$$(\dot{q}_{AI,U})_{ACT} = -(\dot{q}_{ACC,U})_{ACT} = -(f_{ACTC}\, q_{AI,U})/\Delta t_U \quad \text{(S6)}$$

where $\Delta t_U = \Delta z / w_U$ is the time for updraft air to move across a layer .

Several cloud modeling studies (Pinsky and Kahin, 3003; Segal et al., 2003; Yin et al., 2005; Phillips et al., 2007) suggest that supersaturations of a few tenths of a percent or more may be achieved in convective clouds above cloud-base, due to strong adiabatic cooling (from high updraft velocities) and relatively low hydrometeor surface area (due to conversion of cloud droplets to precipitation particles). Ghan et al. (2012) suggest that supersaturation above cloud-base should be diagnosed based on a balance between adiabatic cooling and water vapor condensation onto hydrometeors, but this requires knowledge of both the updraft velocity and hydrometeor size distribution. This information is lacking or very approximate in the current CAM5.0 convective cloud parameterizations, so currently we simply prescribe an above cloud-base supersaturation of 0.3%, based on the several cloud-modeling studies cited above. With this we can calculate the aerosol activation fractions as done in the Abdul-Razzak and Ghan (2000) parameterization.

The in-cloud wet removal tendency for cloud-borne aerosols in the updraft is given by

$$(\dot{q}_{ACC,U})_{WET} = -\lambda_{WETC,U}\, q_{ACC,U} \quad \text{(S7a)}$$

and the wet-removal first-order loss rate is taken to be

$$\lambda_{WETC,U} = RPROD/(A_U\, ICWMR) \quad \text{(S7b)}$$

This gives

$$A_U\,(\dot{q}_{ACC,U})_{WET} = -(RPROD/\,ICWMR)\,q_{ACC,U} \qquad \text{(S7c)}$$

After aerosol mixing ratios in the updrafts and downdrafts have been calculated, changes to the grid-cell mean aerosol mixing ratios are calculated by solving

$$\frac{\partial \bar{q}_{AX}}{\partial t} = -\frac{\partial}{\partial p}\left[M_U\,q_{AX,U} + M_D\,q_{AX,D} + M_E\,q_{AX,E}\right] + A_U(\dot{q}_{AX,U})_{ACT} + A_U(\dot{q}_{AX,U})_{WET} + A_E(\dot{q}_{AX,E})_{RES} \qquad \text{(S8)}$$

The right-most term involves resuspension in the environment of cloud-borne aerosols detrained from the updraft. Currently we assume complete resuspension for the detrained convective-cloud-borne aerosols, so there is no transfer of convective- to stratiform-cloud-borne aerosols.

It is important to note that although the wet removal terms in the previous convective treatment (S1-2) and new convective treatment (S7abc) appear to be rather similar, especially after some algebraic substitutions, they affect grid-cell mean aerosol mixing ratios in very different ways. In the previous treatment, wet removal occurring at mid levels (e.g., 700 hPa) directly reduces grid-cell mean aerosol mixing ratios at that level. In the new unified treatment, wet removal occurring at 700 hPa in the updraft reduces the updraft aerosol flux ($M_U q_{AX,U}$) above this level. This leads to a reduction in grid-cell mean aerosol mixing ratios at detrainment levels. However, because the wet removal sink term in (S8) is approximately balanced by the updraft flux divergence term at 700 hPa, this wet removal will often have little direct impact on grid-cell mean aerosol mixing ratios at 700 hPa.

2. Aerosol and Aerosol-Cloud Processes in the CAM5

We use a developmental version of the stand-alone CAM5, which has nearly identical physics to the released version CAM5.1. Aerosol evolution in CAM5 is controlled by a

combination of emission, transport, aerosol microphysics (new particle formation, condensation, coagulation, aging, etc.), and dry and wet removal. Aerosol and cloud microphysics and their interactions are described and evaluated by Liu et al. (2012). Here we briefly summarize the processes in CAM5 that are relevant to aerosol (BC in particular) and evolution.

1) Aerosol Mixing State and Aging

CAM5 employs a modal aerosol module (MAM) to represent aerosols (Liu et al., 2012). The aerosol mixing-state and size distribution is represented by multiple log-normally distributed modes, with internal mixing assumed for aerosol species [e.g., sulphate, BC, primary organic matter (POM), secondary organic aerosol (SOA)] within each individual mode. Two versions of MAM are used in this study: a 3-mode "fast" representation (MAM3) and a more complex 7-mode "benchmark" representation (MAM7). The major difference between MAM3 and MAM7 related to BC lies in the treatment of aging. In MAM3, BC and POM are emitted into the accumulation mode, which also contains highly-hygroscopic sulphate and sea-salt and moderately hygroscopic SOA. The freshly emitted BC and POM are thus immediately mixed with these hygroscopic species in particles that can be viable cloud condensation nuclei (CCN), depending on the amount of BC/POM emissions versus existing sulphate/sea-salt/SOA. In MAM7, BC and POM are emitted into a primary carbon mode, which contains no other species. The hygroscopicity of this mode depends on the assumed POM hygroscopicity which is generally lower than that of the MAM3 accumulation mode. Thus in MAM7, the freshly emitted BC and POM are in particles that are less-viable CCN and less likely to experience wet removal. As hygroscopic species (e.g., H_2SO_4, NH_3 and semi-volatile organic vapors) condense onto primary carbon mode particles, the particles are "aged" (become more hygroscopic) and are gradually transferred into the MAM7 accumulation mode. The rate of transfer is controlled by

145 somewhat uncertain aging parameters, such as the number of mono-layers of sulphate coating
146 needed to make a fresh BC/POM particle a viable CCN (Liu et al. 2012).
147 *2) Aerosol-Cloud Interactions*
148 In CAM5, aerosol particles are assumed to either be suspended in the air or reside in cloud
149 droplets, and these are referred to as interstitial and cloud-borne aerosol, respectively. Particles
150 that are viable CCN and are within the cloudy portion of a grid cell are converted from the
151 interstitial state to the cloud-borne state through aerosol activation (or nucleation scavenging).
152 Cloud-borne aerosols in stratiform clouds are treated prognostically in CAM5: their mixing
153 ratios are saved between model time steps and evolve as a result of source, sink, and transport
154 processes. Their activation is parameterized using vertical velocity (resolved and sub-grid
155 turbulent) and aerosol properties of all the modes following Abdul-Razzak and Ghan (2000).
156 Activation may occur when aerosols are carried into clouds from below and when cloud fraction
157 increases. Therefore, liquid cloud fraction diagnosed from the triangular distribution of grid-
158 mean relative humidity in CAM5 is critical to aerosol activation. Cloud-borne aerosols in
159 convective clouds are treated diagnostically: their mixing ratios are diagnosed each model time
160 step (with no "memory") from the interstitial aerosol mixing ratios. Cloud-borne BC particles are
161 returned to the interstitial state upon drop evaporation (i.e., resuspension). The representation of
162 activation/resuspension processes, and consequent effects on clouds and precipitation in the
163 model, has direct and indirect impacts on BC wet removal and transport.
164 *3) Removal*
165 Both interstitial and cloud-borne aerosol particles are subject to wet and dry removal
166 (deposition). CAM5 treats in-cloud and below-cloud wet removal of aerosols. In-cloud wet
167 removal involves activation of interstitial aerosol to become cloud-borne, followed by

conversion of cloud droplets (and the cloud-borne aerosol particles) to precipitation. The activation step is described above. The removal rate of cloud-borne aerosol is equal to the rate at which cloud-water is converted to precipitation, as determined by the model's cloud parameterizations. In-cloud wet removal through attachment of interstitial aerosol to ice particles followed by conversion of ice particles to precipitation is currently not treated. Below-cloud wet removal involves direct capture of interstitial aerosols by precipitation particles through a number of processes (e.g., inertial impaction, Brownian diffusion) and is relatively inefficient for aerosol in the accumulation mode size range. Different tunable parameters, which we refer to as wet-removal adjustment factors (≤ 1), are applied to the calculation of the stratiform/convective in-cloud and below-cloud scavenging rates to account for various uncertainties from the aerosol mixing state, activation, and model-predicted cloud and precipitation properties (Liu et al., 2012). When raindrops evaporate below cloud, a portion of the wet-scavenged aerosol is resuspended as interstitial particles and this produces some downwards redistribution of aerosols.

For BC and sulphate (predominately sub-micron) in CAM5, dry removal accounts for about 16-18% and 11-12% of the total removal on a global annual basis (with the ranges reflecting MAM3 and MAM7 values). Aerosol dry deposition velocities are calculated using the method developed by Zhang et al. (2001) with model provided aerodynamic resistance, friction velocity, and surface properties. Gravitational settling is also treated.

4) Transport

Interstitial aerosol particles in CAM5 are transported by resolved winds, turbulence, and shallow and deep convection. Advection by resolved winds is neglected for cloud-borne aerosols due to the assumption that aerosol particles in liquid clouds are relatively short-lived (Koch et al., 2006). Stratiform-cloud-borne aerosols undergo turbulent vertical transport. Ghan and Easter

(2006) showed that neglecting transport of stratiform-cloud-borne aerosols by resolved winds introduces small global mean biases in aerosol number concentrations at a coarse resolution (2°×2.5°). Ma et al. (2012) have compared CAM5 simulations allowed to evolve freely with simulations constrained by various reanalysis products and found that CAM5 Arctic circulation patterns (mean and transient eddy) are quite reasonable. This suggests that transport of aerosols by resolved winds in CAM5 is not a major contributor to the poor simulation of remote Arctic aerosols.

3. Sensitivity test on Emissions

The simulations discussed in the main text use the IPCC AR5 emissions for year 2000. The AR5 BC emissions for 1980 are quite different from the 2000 emissions due to a number of socio-economic changes. Although the global annual emissions are lower for 1980 (6.9 Tg C yr^{-1}) than for 2000 (7.8 Tg C yr^{-1}), more importantly for the Arctic, as shown in Fig. S1, the DJF emissions integrated between 40°N and 70°N were significantly higher in 1980 than in 2000 (1.87 vs. 1.25 Tg C yr^{-1}). At these latitudes, the summer (JJA) BC emissions are higher than winter due to wildfire emissions. This summer increase is lower in 1980 than in 2000 (the ratios of JJA to DJF emissions for 40-70°N are 1.12 and 1.46 respectively), and this could make a difference to the seasonal cycle of Arctic BC. It should be noted that the AR5 SO_2 emissions for years 1980 and 2000 have the similar difference in DJF between 40°N and 70°N (113% higher emission in 1980; figure not shown).

Figure S2 compares simulated DJF BC in two identical simulations (based on the ALL_m7 configuration) but with the 1980 emissions and 2000 emissions, respectively. The zonal-mean BC burden is smaller in the 1980 simulation south of 40°N (consistent with the distribution of BC emissions) but is larger (by a factor of 1.5) from 50°N to 90°N. Previous studies have

identified N. Europe and Russia as major source regions for Arctic haze (Shindell et al., 2008; Matsui et al., 2011), and the large 1980 to 2000 emissions change between 40°N and 70°N is likely responsible for the difference in Arctic BC between the two simulations. Larger total burden leads to larger cloud-borne burden and wet deposition flux as well, but the total removal rates are almost identical in the two simulations (see Fig. S2b). The Arctic sulphate burden and surface mixing ratios are doubled under the 1980 emissions scenario due to the even larger increase in SO_2 emission than in 2000 (figure not shown).

With the 1980 emission, the predicted surface BC and sulphate seasonality over the Arctic sites is further improved. This is because of the stronger DJF sources between 40°-70°N in the 1980 emission inventory than in the 2000's, which more effectively increases the Arctic BC and sulphate mixing ratios (from the surface to about 600 hPa) than sources from lower latitudes.

4. Tables for model-observation comparison

Table S1 summarizes how the modifications to CAM5 impact the simulated surface-level BC compared to observations from three networks/compilations. In Liu et al. (2011b) and Wang et al. (2011a), simulated BC are compared to observations from the IMPROVE and EMEP networks and the combined compilations of Liousse et al. (1996) and Cooke et al. (1999). Table S1 lists the multi-site means and medians for these three datasets and additionally for the Zhang et al. (2008) China dataset. The changes between the various simulations are considerably smaller at these surface sites than the changes to the global annual burdens (Table 2 in the text). This is not surprising for the IMPROVE and EMEP networks, where the sites are in the continental US and Europe, relatively close to sources. The slower BC aging has small impacts for the same reasons. The unified convection treatment lowers the simulated values at the sites slightly, although it increases the global burden. The simulation with 1980 emissions has

noticeably higher mixing ratios over the IMPROVE and EMEP network sites because of emissions changes in these regions. The simulated values for the base model configurations are lower than observed, so model changes that increase BC burden and transport to the Arctic also reduce the CAM5 low-bias for these datasets. All the simulations strongly underestimate the China observations from Zhang et al. (2008), suggesting that BC emissions for this region may be significantly underestimated. One of the most notable features is that the MMF simulation gives much lower surface mixing ratios for the three datasets than the CAM5std and the CTRL simulation, although the MMF global burden is about 50% higher. As shown in the BC vertical distributions (see Figs. 9, 10 and 11), CAM5 often predicts a stronger near-surface peak than the MMF at low- and mid-latitudes, suggesting stronger boundary-layer turbulent mixing and vertical transport in the MMF. Correlation coefficients (not shown) vary only slightly between the simulations, one exception being the 1980 emissions simulation and EMEP Network, but the correlations are all rather low for that dataset.

Table S2 provides similar information for surface-level sulphate, using observations from the IMPROVE, EMEP, and U. Miami (marine sites) networks. The changes between the various simulations are larger than those for BC, but the changes are still smaller than the global annual burden changes. As with BC, the changes increase sulphate mixing ratios, which increase the high bias for the IMPROVE and EMEP continental sites, but improve (and even reverse) the low bias for the U. Miami remote marine sites. The new unified convection (CONV) increases surface mixing ratios, compared to the slight decrease for BC, which we attribute to their different sources (locations and primary vs. secondary). Correlation coefficients again vary only slightly between the simulations, except for the 1980 emissions simulation and EMEP Network.

References (for Supplementary Material):

Abdul-Razzak, H., and S. J. Ghan: A parameterization of aerosol activation 2. Multiple aerosol types, *J. Geophys. Res.-Atmos.*, 105(D5), 6837–6844, 2000.

Bond, T. C., Bhardwaj, E., Dong, R., Jogani, R., Jung, S. K., Roden, C., Streets, D. G., and Trautmann, N. M.: Historical emissions of black and organic carbon aerosol from energy-related combustion, 1850–2000, *Global Biogeochem. Cy.*, 21(2), Gb2018, doi:10.1029/2006gb002840, 2007.

Cooke,W. F., C. Liousse, H. Cachier, and J. Feichter (1999), Construction of a 1 degrees×1 degrees fossil fuel emission data set for carbonaceous aerosol and implementation and radiative impact in the ECHAM4 model, *J. Geophys. Res*., 104, 22137–22162.

Ghan, S. J. and Easter, R. C.: Impact of cloud-borne aerosol representation on aerosol direct and indirect effects, *Atmos. Chem. Phys.*, 6, 4163-4174, doi:10.5194/acp-6-4163-2006, 2006.

Koch, D., Schmidt, G. A., and Field, C.: Sulfur, sea salt and radionuclide aerosols in GISS ModelE, *J. Geophys. Res.*, 111, D06206, doi:10.1029/2004/JD005550, 2006.

Liousse, C., et al.: A global three-dimensional model study of carbonaceous aerosols, *J. Geophys. Res.*, 101, 19411–19432, 1996.

Neale, R. B., Chen, C.-C., Gettelman, A., Lauritzen, P. H., Park, S., Williamson, D. L., Conley, A. J., Garcia, R., Kinnison, D., Lamarque, J.-F., Marsh, D., Mills, M., Smith, A. K., Tilmes, S., Vitt, F., Cameron-Smith, P., Collins, W. D., Iacono, M. J., Easter, R. C., Ghan, S. J., Liu, X., Rasch, P. J., and Taylor, M. A.: Description of the NCAR Community Atmosphere Model (CAM 5.0), NCAR/TN–???+STR, 2010.

Park, S., and C. S. Bretherton: The University of Washington shallow convection and moist turbulence schemes and their impact on climate simulations with the Community Atmosphere Model, *J. Climate*, 22(12), 3449–3469, doi:10.1175/2008jcli2557.1, 2009

Phillips, V. T. J., L. J. Donner, and S. T. Garner: Nucleation processes in deep convection simulated by a cloud-system-resolving model with double-moment bulk microphysics, *J Atmos Sci*, *64*(3), 738-761, 2007.

Pinsky, M. B., and A. P. Khain: Effects of in-cloud nucleation and turbulence on droplet spectrum formation in cumulus clouds, *Q J Roy Meteor Soc*, *128*(580), 501-533, 2002.

Segal, Y., M. Pinsky, A. Khain, and C. Erlick: Thermodynamic factors influencing bimodal spectrum formation in cumulus clouds, *Atmos Res*, *66*(1-2), 43-64, 2003.

Yin, Y., K. S. Carslaw, and G. Feingold: Vertical transport and processing of aerosols in a mixed-phase convective cloud and the feedback on cloud development, *Q J Roy Meteor Soc*, *131*(605), 221-245, 2005.

Yttri, K. E., et al.: Elemental and organic carbon in PM_{10}: a one year measurement campaign within the European Monitoring and Evaluation Programme EMEP, *Atmos. Chem. Phys.*, 7, 5711-5725, doi:10.5194/acp-7-5711-2007, 2007.

Zhang, G. J., and N. A. McFarlane: Sensitivity of climate simulations to the parameterization of cumulus convection in the Canadian Climate Center general-circulation model, *Atmos. Ocean*, 33(3), 407–446, 1995.

Zhang, L. M., Gong, S. L., Padro, J., and Barrie, L.: A size-segregated particle dry deposition scheme for an atmospheric aerosol module, *Atmos. Environ.*, 35(3), 549–560, 2001.

Zhang, X. Y., et al.: Carbonaceous aerosol composition over various regions of China during 2006, *J. Geophys. Res*., 113, D14111, doi: 10.1029/2007JD009525, 2008.

Zipser, E. J., and M. A. Lemone: Cumulonimbus Vertical Velocity Events in Gate. Part II: Synthesis and Model Core Structure, *J. Atmos. Sci.*, *37*, 2458-2469, 1980.

Table S1: Observed and simulated multi-site mean and median BC (in ng m^{-3}, with medians in parentheses) for IMPROVE network sites (annual means), EMEP network sites (annual means), Zhang et al. (2008) China sites, and Liousse et al. (1996) and Cooke et al. (1999) compilations (various time periods; L96&C99). The IMPROVE, EMEP, and Liousse-Cooke sites correspond to Figures 11a, 11b, and 13b of Liu et al. (2011b), respectively.

Case	**IMPROVE**	**EMEP***	**China****	**L96&C99**
Observed	257. (215.)	730. (620.)	3015. (3600.)	398. (123.)
MMF	148. (119.)	295. (290.)	652. (614.)	179. (47.)
CAM5std	206. (153.)	410. (391.)	891. (854.)	242. (61.)
CTRL	214. (158.)	423. (413.)	948. (914.)	256. (51.)
CONV	214. (160.)	409. (397.)	906. (882.)	242. (57.)
CONV_sact	209. (156.)	396. (387.)	918. (885.)	239. (65.)
CONV_FD	215. (166.)	422. (400.)	950. (905.)	247. (74.)
CONV_SF	218. (166.)	435. (416.)	968. (901.)	257. (67.)
CONV_m7	226. (170.)	430. (409.)	990. (914.)	260. (66.)
ALL_m3	222. (172.)	436. (412.)	967. (904.)	252. (64.)
ALL_m7	238. (190.)	476. (424.)	1049. (995.)	277. (75.)

* The 2 "urban background" sites (see Table 1 of Yttri et al., 2007) are excluded.
** The 5 sites in the "urban group" (see Table 2 of Zhang et al., 2008) are excluded.

Table S2: Observed and simulated multi-site means and medians for annual average sulphate (in μg m^{-3}, with medians in parentheses) for IMPROVE, EMEP, and University of Miami network sites. The IMPROVE, EMEP, and U. Miami sites correspond to Figures 9a, 9b, and 10 of Liu et al. (2011b), respectively.

Case	IMPROVE	EMEP	U. Miami
Observed	1.59 (0.98)	2.37 (2.18)	0.94 (0.43)
MMF	2.17 (1.81)	2.64 (2.80)	1.01 (0.61)
CAM5std	2.06 (1.63)	2.27 (2.39)	0.63 (0.35)
CTRL	2.23 (1.74)	2.44 (2.50)	0.68 (0.35)
CONV	2.37 (1.90)	2.52 (2.59)	0.83 (0.49)
CONV_sact	2.30 (1.85)	2.39 (2.48)	0.81 (0.42)
CONV_FD	2.44 (1.92)	2.62 (2.67)	0.87 (0.50)
CONV_SF	2.59 (2.05)	2.79 (2.94)	0.93 (0.54)
CONV_m7	2.44 (1.87)	3.10 (3.31)	0.87 (0.52)
ALL_m3	2.60 (2.00)	2.84 (2.92)	0.89 (0.54)
ALL_m7	2.74 (2.04)	3.64 (3.92)	0.97 (0.59)

Table S3: Observed (as listed in Table 1 of Wang et al., 2011b) and simulated global annual mean LWP, total precipitation rate (PRECT), residual fluxes at surface (RESSURF) and top of the model atmosphere (RESTOM) and cloud forcing (SWCF and LWCF).

Case	**LWP** ($g\ m^{-2}$)	**IWP** ($g\ m^{-2}$)	**PRECT** ($mm\ d^{-1}$)	**SWCF** ($W\ m^{-2}$)	**LWCF** ($W\ m^{-2}$)
Observed	(50,87)	-	2.61	(–46, –53)	(27, 31)
MMF	55.88	9.87	2.85	–50.48	25.96
CAM5std	41.15	17.77	2.96	–49.12	23.67
CTRL	41.04	17.17	2.98	–48.19	22.78
CONV	47.02	17.30	2.95	–51.42	23.78
CONV_sact	46.22	17.79	2.94	–52.06	24.74
CONV_FD	47.30	17.19	2.93	–50.17	23.60
CONV_SF	48.82	17.46	2.94	–52.00	24.03
CONV_m7	46.84	16.94	2.93	–50.64	23.40
ALL_m3	48.62	17.76	2.92	–51.60	24.84
ALL_m7	48.13	17.46	2.90	–50.69	24.39

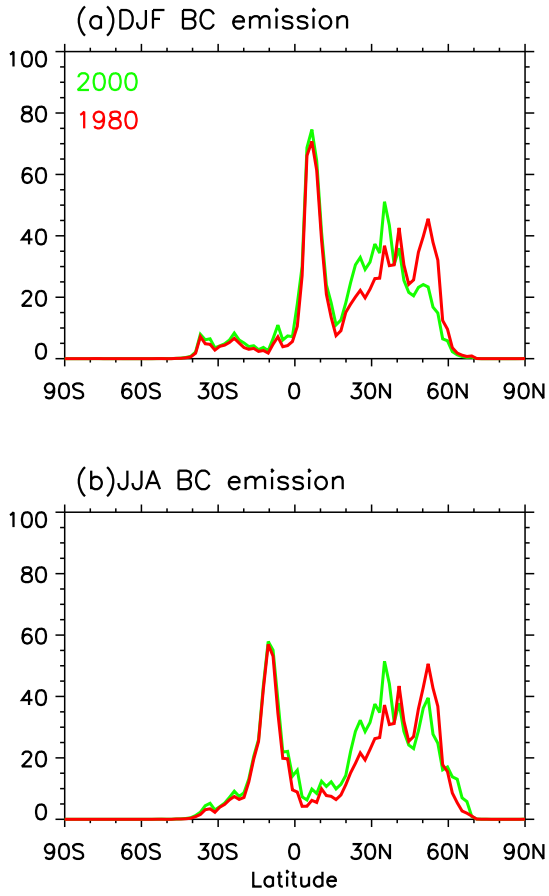

Figure S1: Seasonal zonal-mean BC emission rates (kg C km^{-2} yr^{-1}) for the year of 2000 and 1980 in (a) DJF and (b) JJA months.

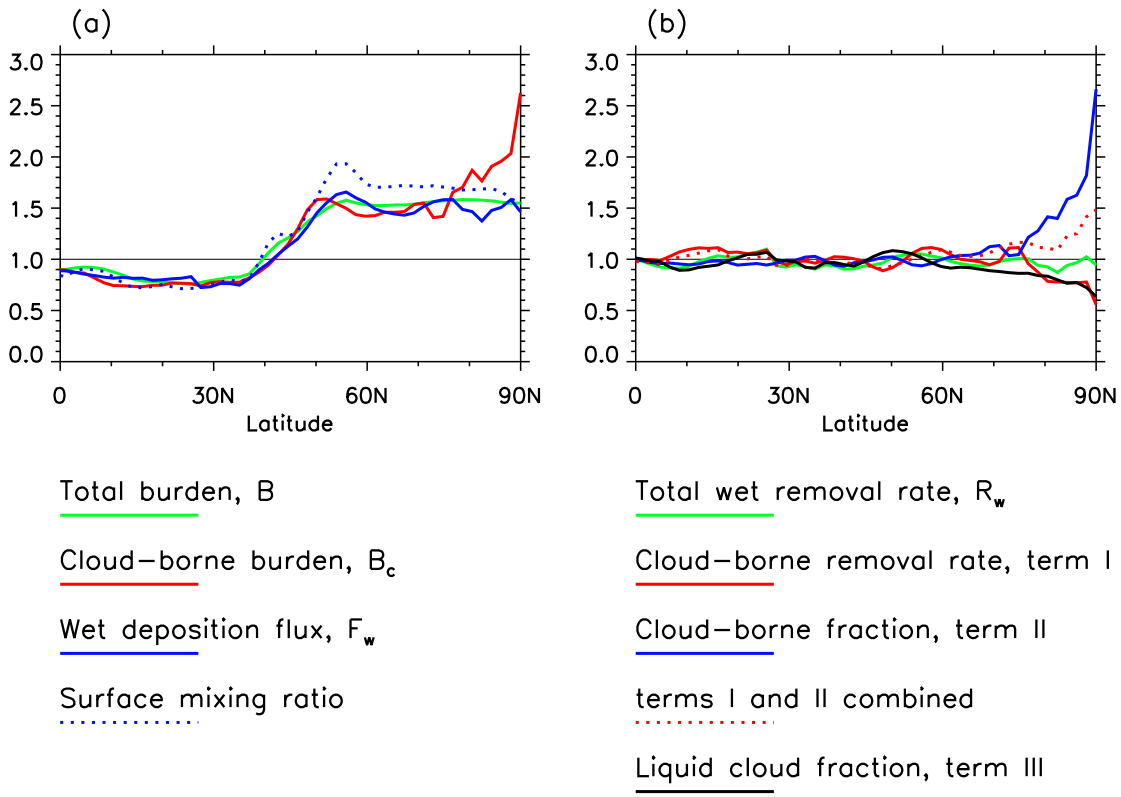

Figure S2: the ratios of the quantities related to BC burden and wet removal, as described in Eqs. (1-3) in the text, derived from two CAM5 simulations (close to the ALL_m7 setup) with year 1980 emissions and 2000 emissions respectively. Quantities are averaged zonally and over the Northern Hemisphere winter months (DJF).